Available online at https://link.springer.com/journal/42241
http://www.jhydrodynamics.com
Journal of Hydrodynamics, 2025
https://doi.org/10.1007/s42241-025-0007-4

A novel hull form optimization framework based on multi-fidelity deep neural network

Ya-bo Wei[1], Guo-hua Pan[2], Passakorn Paladaechanan[1], De-cheng Wan[1*]
1. *Computational Marine Hydrodynamics Lab (CMHL), School of Naval Architecture, Ocean and Civil Engineering, Shanghai Jiao Tong University, Shanghai 200240, China*
2. *Ningbo Pilot Station, Ningbo Dagang Pilotage Co., Ltd., Ningbo 315020, China*

(Received November 15, 2024, Revised November 25, 2024, Accepted November 26, 2024, Published online April 17, 2025)

Abstract: With the advancements in computer technology, the simulation-based design (SBD) technology has emerged as a highly effective method for hull form optimization. The SBD approach often employs various methods to evaluate the hydrodynamic performance of the sample ships. Although the surrogate model is applied to SBD method to replace time-consuming evaluation, many high-fidelity data are typically required to guarantee the accuracy of the surrogate model, resulting in significant computational costs. To improve the optimization efficiency and reduce computational burdens, we propose a novel hull form optimization framework utilizing the multi-fidelity deep neural network (MFDNN), leveraging multi-source data fusion and transfer learning. This framework constructs an accurate multi-fidelity surrogate model which correlates design parameters with hydrodynamic performance of the hull by blending data with different fidelity. Besides, computational fluid dynamics (CFD) evaluations based on viscous flow are served as the high-fidelity model, while potential-theory evaluations represent the low-fidelity model. Then, this framework is validated using mathematical functions to prove its practicability in optimization. Finally, the optimization design of the resistance of the DTMB-5415 ship is carried out. Our findings demonstrate that this framework can take into account both efficiency and accuracy, which is preferable in optimization tasks. The optimized hull form obtained by the framework has better resistance performance.

Key words: Computational fluid dynamics (CFD), hull form optimization, surrogate model, MFDNN, data fusion, DTMB-5415 ship

0. Introduction

In recent years, the computer technology has led to the widespread application of Computational Fluid Dynamics (CFD) in the field of naval architecture and ocean engineering. The simulation-based design (SBD) method, developed on this basis, has introduced a transformative approach to hull form optimization[1]. This method has attracted wide attention since it was proposed. It is globally recognized as a powerful tool for hull form optimization[2] currently. In SBD-based hull form optimization, the surrogate model replaces the time-consuming CFD evaluations, which can reduce the computational costs and improve the optimization efficiency. It is an effective way to promote the application of CFD technology to hull form optimization design. At present, the common surrogate model mainly includes support vector machine (SVM), Kriging model, radial basis function (RBF) model, artificial neural network (ANN), etc.[3-6]. In the optimization process, the evaluation of the objective function is replaced by a surrogate model instead of a high-precision CFD evaluation to improve the optimization efficiency. Therefore, the accuracy of the surrogate model is particularly important, which its reliability can be improved by cross-validation (CV) and reducing the variance of the model[7].

Scholars have applied the SBD approach to hull optimization tasks. Feng et al.[8] applied the SVM to optimize the resistance and wake circumferential nonuniformity of an offshore aquaculture vessel with 60 sample points. The optimal hull was obtained by non-dominated sorting genetic algorithm II (NSGA-II). Compared with the model tests, the results showed that the resistance and wake circumferential nonuniformity of the optimal hull were reduced by 1.59%, 17.80%. Tahara et al.[9] designed an optimization framework to minimize the resistance of a fast multihull ship. A Kriging model was constructed to

Project supported by the National Natural Science Foundation of China (Grant No. 52131102).
Biography: Ya-bo Wei (1996-), Male, Ph. D. Candidate,
E-mail: wyb2538@163.com
Corresponding author: De-cheng Wan,
E-mail: dcwan@sjtu.edu.cn

improve the optimization efficiency. The optimal hull was compared and confirmed by the experimental measurements. Liu et al.[10] optimized the resistance performance of the Wigley hull based on the Kriging model. A bulbous bow was generated by the deformation method using radial basis functions (RBF). The single-objective genetic algorithm was employed to obtain the optimal hull form. It was found that the resistance of the optimal hull was reduced by 11.7 %. Huang et al.[11] used an RBF surrogate model to optimize the resistance and seakeeping performance of Series 60 hull. Diez et al.[12] constructed an RBF surrogate model to optimize the resistance and seakeeping performance of Delft catamaran under stochastic conditions. Coppedè et al.[13] proposed a computational framework for hydrodynamic shape optimization based on the Kriging model. The framework was then applied to optimize the resistance of KCS ship. The results showed that the resistance of optimal hull was reduced by 4%. Besides, ANN-based surrogate models were also applied to optimize the resistance performance of Wigley hull[14]. The results showed that the combination of ANN and genetic algorithm provided a practical and efficient optimization tool. Hou[15] used an ANN surrogate model to optimize the Wigley hull.

In the process of constructing the surrogate models mentioned above, the performance of each sample ship was evaluated by the same solver. Thus, the surrogate model constructed by the evaluation results is referred to as single-fidelity surrogate models[16]. On the contrary, the surrogate models constructed by the evaluation results of different fidelity solvers are termed as multi-fidelity surrogate models. For the practical engineering optimization problems, especially for complex optimization problems, a large number of sampling points are needed to construct an accuracy surrogate model, which could be extremely resource demanding. Therefore, the optimization efficiency is restricted. To tackle this problem, some researchers proposed the multi-fidelity surrogate model by using a portion of low-fidelity (LF) samples combining with high-fidelity samples to accelerate the optimization process. For optimization problems, a commonly used multi-fidelity surrogate model is the Co-Kriging model which was developed based on the Kriging model[17]. Kennedy and O'Hagan[18] proposed the Co-Kriging model based on Gaussian process by establishing the relationship between low-fidelity and high-fidelity samples. Forrester et al.[19] firstly applied the Co-Kriging model to engineering optimization problem. On this basis, Liu et al.[20] used the Co-Kriging model to optimize the resistance and wake performance of the JBC ship. The coarse mesh evaluation results are used as the low-fidelity samples and the fine mesh evaluation results are used as the high-fidelity samples. Compared with the Kriging model constructed by 60 high-fidelity samples, the Co-Kriging model only used 30 high-fidelity samples and 60 low-fidelity samples. The total computational time was reduced by 25% while obtaining better-performing hulls. Scholcz and Klinkenberg[21] applied the adaptive multi-fidelity Kriging based on the augmented expected improvement function to optimize the resistance of DTMB-5415. The results showed that the adaptive multi-fidelity Kriging model could use less samples to obtain a better shape. However, the construction process of a Co-Kriging model is complex, and the construction cost is high[17]. Besides, the multi-fidelity Kriging surrogate model struggles with the high dimensional and strongly nonlinear problems[22], it is necessary to construct a simple multi-fidelity sample fusion method with high precision.

With the advancements in artificial intelligence, the deep neural network (DNN) is widely applied in flow field reconstruction/prediction and flow control tasks[23-24]. In this paper, to improve the efficiency and reduce the computation cost, especially in complex optimization problems, we propose a novel multi-fidelity hull form optimization framework based on the multi-fidelity deep neural network (MFDNN). In the framework, the MFDNN surrogate model is used to replace the time-consuming CFD evaluation by combining low-fidelity and high-fidelity data. The reliability of this framework is verified using mathematical optimization functions. Subsequently, our framework is applied to optimize the resistance of DTMB-5415 at $Fr = 0.28$, and the results are compared with the results obtained by traditional single high-fidelity Kriging model.

1. Hull form optimization framework based on multi-fidelity deep neural network

1.1 *Optimization framework*

In the process of hull form optimization, high-fidelity CFD evaluation data is often used to construct the surrogate model, which will seriously restrict the efficiency of hull form optimization. To tackle this problem, we propose a novel optimization framework based on MFDNN. As shown in Fig. 1, the new hull form optimization framework consists of the Sobol method which is the design of experiment method, CFD evaluation and MFDNN surrogate model. The process of the novel optimization framework is presented as follows:

(1) The design variables are decided by designers and the number of design variables is d. $10d$ low-fidelity and d high-fidelity sample points are selected at once using the Sobol sampling method.

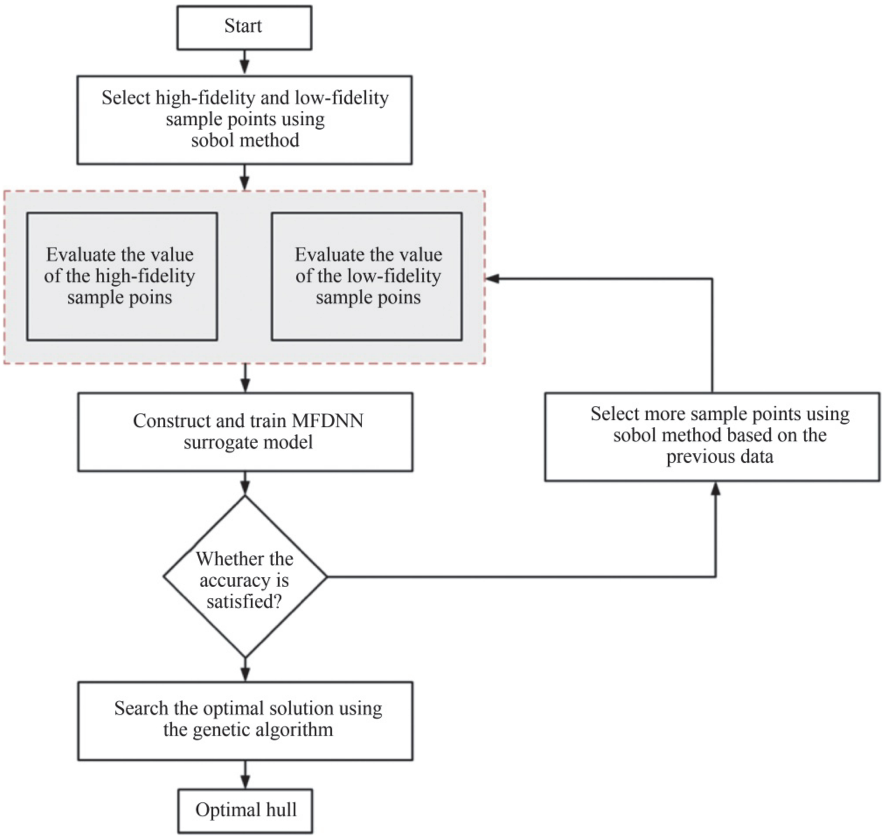

Fig. 1 Hull form optimization framework based on MFDNN

The introduction to Sobol method can be found in Section 1.3.

(2) Low-fidelity CFD solver and high-fidelity CFD solver are employed to evaluate the hydro-dynamic performance of low-fidelity sample points and high-fidelity sample points. In this paper, the potential solver evaluation results are selected as the low-fidelity results and the viscous solver evaluation results are selected as the high-fidelity results.

(3) The MFDNN surrogate model is constructed using high-fidelity sample points and low-fidelity sample points.

(4) Evaluate the accuracy of MFDNN surrogate model. If the accuracy of the MFDNN surrogate model is not satisfied, more sample points will be selected using the Sobol sampling method. Repeat step (2).

(5) Search the optimal solution using genetic algorithm and output the optimal hull.

1.2 *Multi-fidelity deep neural network (MFDNN) surrogate model*

In this section, the MFDNN surrogate model is applied to the hull form optimization framework to construct a more accurate surrogate model by integrating low-fidelity sample data and high-fidelity sample data. In the study of MFDNN, the main problem is how to construct the relationship between high and low fidelity sample data. Based on the autoregressive method, Kennedy et al.[18] expressed the relationship between high-low fidelity samples as

$$\boldsymbol{f}_{\mathrm{H}} = k\boldsymbol{f}_{\mathrm{L}} + z(\boldsymbol{x}) \tag{1}$$

where $\boldsymbol{f}_{\mathrm{H}}$ is the high-fidelity sample data, $\boldsymbol{f}_{\mathrm{L}}$ is the low-fidelity sample data, k is the scaling factor and $z(\boldsymbol{x})$ is the data noise.

It can be seen from Eq. (1) that this method performs well when dealing with the linear correlation between low-fidelity data and high-fidelity data. However, if the nonlinear relationship between high-fidelity and low-fidelity data is significant, this method becomes unsuitable.

In order to tackle the above problems, Meng et al.[25] proposed a generalized autoregressive method to address both linear and nonlinear relationships between high and low fidelity data

$$\boldsymbol{f}_{\mathrm{H}} = \beta F_{\mathrm{L}}(\boldsymbol{x}_{\mathrm{H}}, \boldsymbol{f}_{\mathrm{L}}) + (1-\beta) F_{\mathrm{NL}}(\boldsymbol{x}_{\mathrm{H}}, \boldsymbol{f}_{\mathrm{L}}) \tag{2}$$

where β is a hyperparameter with a value range $[0,1]$, $\boldsymbol{x}_{\mathrm{H}}$ is the high-fidelity data, $\boldsymbol{f}_{\mathrm{L}}$ is the low-fidelity neural network prediction value, $\boldsymbol{f}_{\mathrm{H}}$ is the high-fidelity neural network prediction value, $F_{\mathrm{L}}(\boldsymbol{x}_{\mathrm{H}}, \boldsymbol{f}_{\mathrm{L}})$ is the linear term and $F_{\mathrm{NL}}(\boldsymbol{x}_{\mathrm{H}}, \boldsymbol{f}_{\mathrm{L}})$ is the nonlinear term.

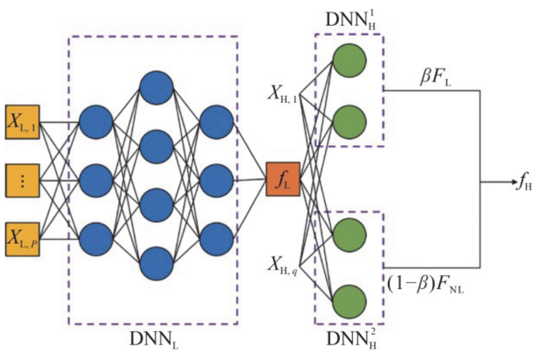

Fig. 2 Architecture of MFDNN

The MFDNN structure is shown in Fig. 2. In Fig. 2, the MFDNN network is composed of three groups of fully connected deep neural networks, which are $\mathrm{DNN_L}$, $\mathrm{DNN_H^1}$, $\mathrm{DNN_H^2}$. Among them, each group deep neural network is composed of input neurons, hidden neurons and output neurons.

The low-fidelity deep neural network structure $\mathrm{DNN_L}$ is shown in Fig. 3. In this network, the low-fidelity data samples $X_{L,1}, \cdots, X_{L,p}$ are input to the low-fidelity deep neural network. The high-fidelity deep neural network structure is shown in Fig. 4, including two fully connected deep neural networks $\mathrm{DNN_H^1}$, $\mathrm{DNN_H^2}$. $X_{H,1}, \cdots, X_{H,q}$ are the high-fidelity sample data. According to Fig. 3, Eq. (2), it can be seen that the high-fidelity data combined with the predicted value from the low-fidelity neural network are fed into $\mathrm{DNN_H^1}$ to approximate the linear term, and into $\mathrm{DNN_H^2}$ to approximate the nonlinear term.

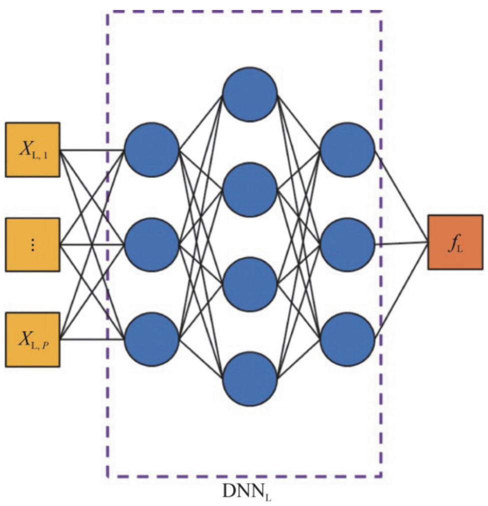

Fig. 3 Architecture of the low-fidelity deep neural network

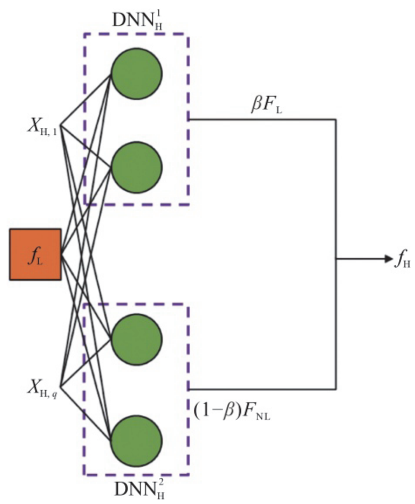

Fig. 4 Architecture of the high-fidelity deep neural network

In the initial stage of neural network training, the parameters in the network are randomly generated. At this time, the difference between the predicted value of the neural network and the true value corresponding to the sample data is large. In order to reduce this difference, the loss function is defined as shown in Eqs. (3)-(5). When the loss function is large, the adaptive moment estimation (Adam) method is used to optimize the parameters until the loss function value is stable[22].

$$MSE_{f_{\mathrm{L}}} = \frac{1}{M_{f_{\mathrm{L}}}} \sum_{j=1}^{M_{f_{\mathrm{L}}}} \left(\left| \boldsymbol{f}_{\mathrm{L}}^{*} - \boldsymbol{f}_{\mathrm{L}} \right|^{2} \right) \tag{3}$$

$$MSE_{f_{\mathrm{H}}} = \frac{1}{M_{f_{\mathrm{H}}}} \sum_{j=1}^{M_{f_{\mathrm{H}}}} \left(\left| \boldsymbol{f}_{\mathrm{H}}^{*} - \boldsymbol{f}_{\mathrm{H}} \right|^{2} \right) \tag{4}$$

$$MSE = MSE_{f_{\mathrm{L}}} + MSE_{f_{\mathrm{H}}} \tag{5}$$

where $MSE_{f_{\mathrm{L}}}$ is the loss function of low-fidelity neural network, $MSE_{f_{\mathrm{H}}}$ is the loss function of high-fidelity neural network, MSE is the loss function of multi-fidelity neural network, $M_{f_{\mathrm{L}}}$ is the number of low-fidelity data samples, $\boldsymbol{f}_{\mathrm{L}}^{*}$ is the true value of low-fidelity data samples, $M_{f_{\mathrm{H}}}$ is the number of high-fidelity data samples and $\boldsymbol{f}_{\mathrm{H}}^{*}$ is the true value of high-fidelity data samples.

1.3 The *Sobol sampling method*

In the process of hull form optimization, the number of sample points is decided by the design of experiments (DOE) method. As one of the experimental design methods, the Sobol method can select the sample points based on the previous sample data, so as to achieve a comprehensive exploration in the design space, which is well-suited for the selection of sample points in the early stage of hull form optimization. Each of its factors is composed of radical inversions with a base number of 2, and the radical inversion of each factor uses a different generating matrix A.

$$X_i := (\Phi_{2,A_1}(i), \cdots, \Phi_{2,A_n}(i)) \tag{6}$$

The radical inversion algorithm can be expressed as:

$$i = \sum_{l=0}^{M-1} a_l(i) b^l \tag{7}$$

$$\Phi_{b.A}(i) = (b^{-1} \cdots b^{-M})[A(a_0(i) \cdots a_{M-1}(i))^{\mathrm{T}}] \tag{8}$$

where b is a positive integer, an integer i is first represented as a number in the base of b, and then a vector is formed by arranging the digits $a_l(i)$ on all the bits of the obtained number, and then multiplied by generator matrix A to produce a new vector. Finally, the new vector is mirrored to the right side of the decimal point, and a number in the range of $[0,1)$ can be obtained. This is the radical inversion operation with b as the base number and A as the generating matrix, which is recorded as $\Phi_{b.A}(i)$.

The Sobol sampling method does not need to determine the number of samples in advance or store the samples. In theory, it can generate infinite as needed. It is well-suited for progressive (or dynamic) sampling. Therefore, the Sobol sampling method is widely used in many optimization problems.

2. Verification of the optimization framework using bechmarking cases

In order to test the reliability of the current optimization framework, the mathematical function is used. The expression of the function is shown in Eq. (9)[26]

$$f_L(x) = \sin(8\pi x), \quad x \in [0,1] \tag{9a}$$

$$f_H(x) = (x - \sqrt{2}) f_L^2(x) \tag{9b}$$

The MFDNN parameter settings during the test are shown in Table 1, where the width in Table 1 represents the number of neurons in each layer of the neural network, and the depth represents the number of hidden layers of the neural network. In addition, the Tanh activation function is used to construct the nonlinear term in $\mathrm{DNN}_{\mathrm{H}}^2$, and the network $\mathrm{DNN}_{\mathrm{H}}^1$ omits the activation function when approximating the linear term of the high-fidelity data.

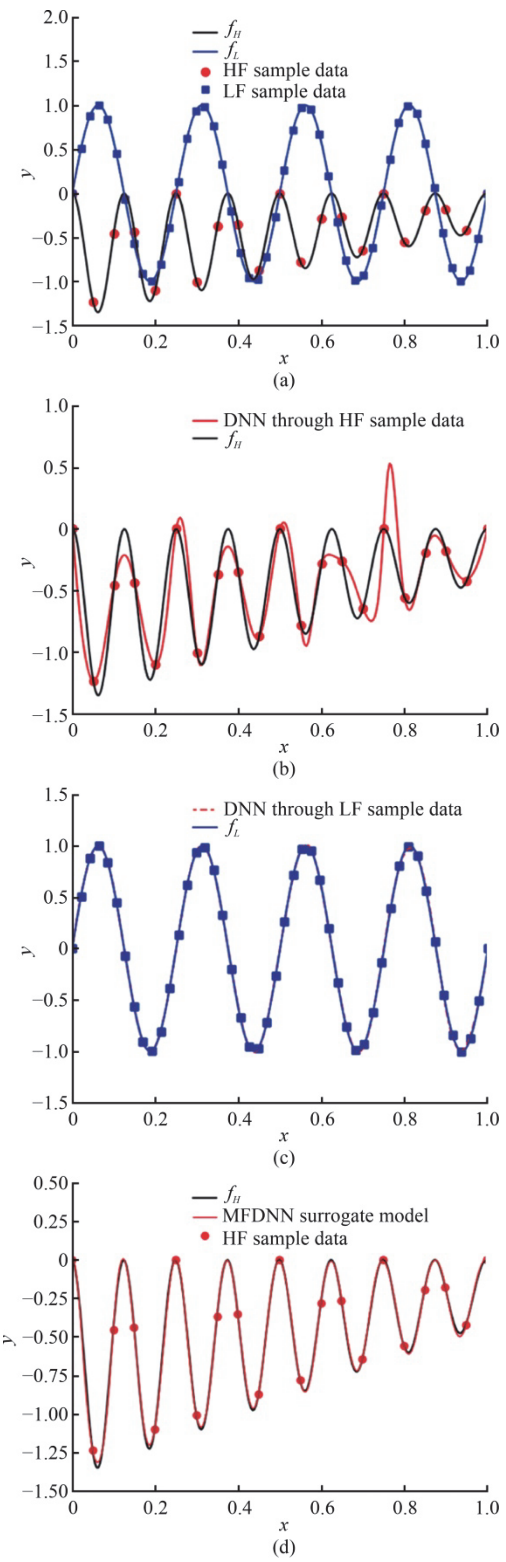

Fig. 5 Mathematical function test results

Table 1 Parameter setting of MFDNN

	Number of neurons in input layer	Width	Depth	Number of neurons in output layer
DNN_L	1	32	3	1
DNN_H^1	2	16	4	1
DNN_H^2	2	16	4	1

Figure 5 shows the test results of mathematical function using the optimization framework proposed in Section 1.1. A total of 21 sets of high-fidelity data and 48 sets of low-fidelity data were selected. Fig. 5(b) shows the comparison between the neural network surrogate model constructed with only high-fidelity data and the true high-fidelity function curve. As shown in Fig. 5(b), when only high-fidelity data is used, the constructed surrogate model is underfitted due to the limited number of sample points. There is a significant difference between the predicted curve and the true function curve. Figure 5(c) compares the neural network surrogate model with only low-fidelity data to the real low-fidelity function curve. As seen from the diagram, the large number of low-fidelity sample data leads to a surrogate model that closely matches the true low-fidelity function curve. Figure 5(d) compares the MFDNN surrogate model constructed by fusing high-fidelity and low-fidelity data. The fused multi-fidelity surrogate model closely matches the true high-fidelity function curve. Compared with the high-fidelity surrogate model in Fig. 5(b), the accuracy is significantly improved after the fusion of a small amount of high-fidelity data with a large amount of low-fidelity data. The reliability of the method is validated using mathematical functions, demonstrating that a more accurate model can be obtained with lower computational cost.

3. Hull form optimization problem for the DTMB-5415

3.1 *Test case description*

In order to further validate the reliability of the proposed framework in practical engineering optimization problems, the resistance of the DTMB-5415 when $Fr = 0.28$ at model scale is optimized based on the proposed optimization framework. As a medium-high speed ship, the DTMB-5415 has rich experiment data and is recognized as the standard ship model in the world. Its three-dimensional model is shown in Fig. 6. The main particulars at model scale can be found in Liu et al.[16].

3.2 *Calculation of ship-hull resistance*

There are two ways to simulate the resistance of DTMB-5415 based on potential flow theory and viscous flow theory. In this paper, the calculation results of the potential flow solver NMShip-SJTU[16] are used as the low-fidelity data and the viscous flow solver naoe-FOAM-SJTU[16] are used as the high-fidelity data.

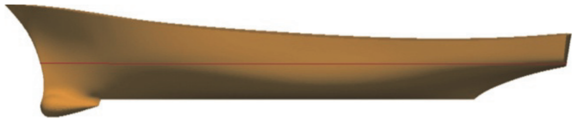

Fig. 6 Geometry model of DTMB-5415

When the NMShip-SJTU solver is used, the wave-making resistance coefficient C_w is directly obtained, and then the viscous resistance coefficient C_f of the ship model is approximately obtained by using the 1957 ITTC plate viscous resistance coefficient formula, as shown in Eq. (10). The two are added and the total resistance R_t of the ship model is obtained according to the dimensional treatment of the length, that is, Eq. (11).

$$C_f = \frac{0.075}{(\lg Re - 2)^2} \tag{10}$$

$$R_t = 0.5(C_f + C_w)\rho U^2 S \tag{11}$$

where Re is the Reynolds number, ρ is the fluid density, U is the ship speed, S is the wet surface of the hull.

Based on NMShip-SJTU, the hull surface mesh and free surface mesh distribution are shown in Fig. 7.

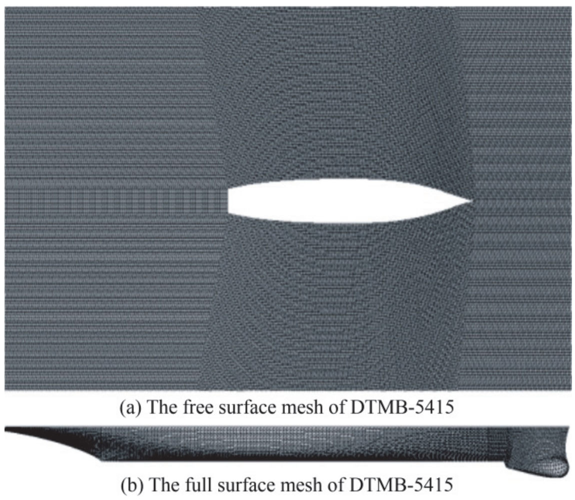

(a) The free surface mesh of DTMB-5415

(b) The full surface mesh of DTMB-5415

Fig. 7 Mesh distribution of the hull surface and free-surface

Based on the NMShip-SJTU solver, the total resistance coefficient is calculated by combining the

Eqs. (10), (11). The comparison between simulation results and experiment results are shown in Table 2. It can be seen from Table 2 that the deviation between the potential flow simulation results and the experimental results is small.

Table 2 Comparison between potential flow calculation result and experimental result

C_w	R_t /N	$R_{t\text{-EFD}}$ /N
1.20×10^{-3}	44.19	44.93

Based on the naoe-FOAM-SJTU solver, the grid convergence verification is conducted. As shown in Fig. 8, three sets of grids with different densities are presented. In this paper, the blockMesh and snappyHexMesh which are the pre-processing tools of OpenFOAM are employed to generate the grid. The blockMesh is used to generate the background mesh and the snappyHexMesh is used to generate the mesh around the hull. On each coordinate axis, there is a $\sqrt{2}$ - old relationship between the background mesh, while other conditions are unchanged.

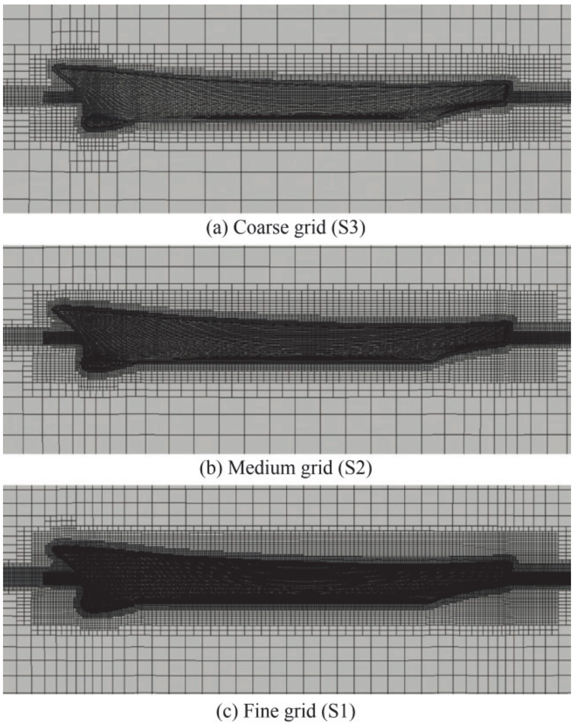

Fig. 8 Computational meshes for convergence analysis

The results of the grid convergence verification are shown in Table 3. The convergence rate R_G is used to measure the convergence of the grid. It can be expressed as

$$R_G = \frac{S_2 - S_1}{S_3 - S_2} \tag{12}$$

In Eq. (11), if $R_G > 1$, the grid convergence is divergent. If $R_G < 0$, the grid convergence is oscillatory. If $0 < R_G < 1$, the grid convergence is monotonic. From Table 3, the value of convergence rate R_G is between 0 and 1, which indicates that the grid convergence is monotonic. Therefore, to accelerate the optimization, the medium grid is used to simulate the resistance of parent and sample ships.

Table 3 Comparison between viscous flow calculation result and experimental result

	Total grid number	R_t
S3	679 061	42.81 N
S2	1 529 295	44.66 N
S1	4 424 945	45.25 N
R_G	-	0.28
EFD	-	44.93 N

In summary, the ship-hull resistance obtained from two different solvers, i.e., potential and viscous flow solvers, are presented and verified.

3.3 *Definition of optimization problem*

In this section, the resistance of the DTMB-5415 ship is optimized, and the free-form deformation (FFD) method[10] is used to transform the shape of sonar dome, as shown in Fig. 9. The shifting method[10] is used to adjust the cross-sectional area curve of the DTMB-5415 along the whole ship.

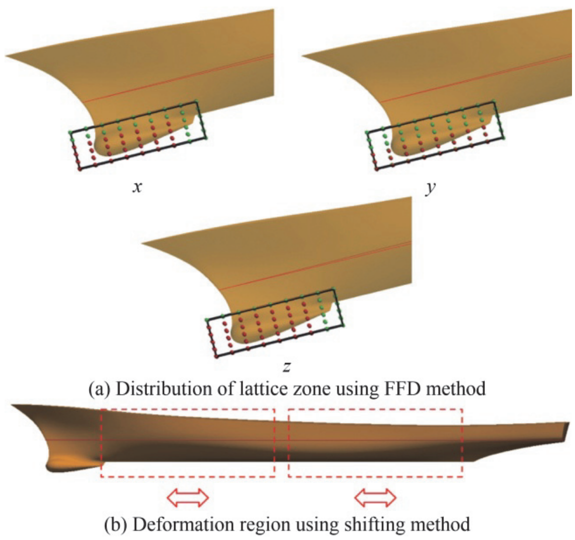

Fig. 9 Bow deformation of DTMB-5415 based on FFD and shifting method

The range of design variables is shown in Table 4, and all variables are dimensionless values along the ship length. Among them, α_{1f}, α_{1a} in the shifting method are the amplitude of the modification function in the shifting method. In Fig. 9, x is the design variable of the red control point moving along the ship length direction, y is the design variable of the red control point moving along the ship width direction, z is the design variable of the red control point moving along the draft direction. According to the relevant literature, the number of sample points is generally 10 times the number of the design variables[4]. In this study, 50 sample points were selected based on the Sobol sampling method, and NMShip-SJTU and naoe-FOAM-SJTU were used as low-fidelity solver and high-fidelity solver.

Table 4 Design variables and their ranges

Method	Design variables	Range
Shifting method	α_{1f}	[−0.016,0.016]
	α_{1a}	[−0.016,0.016]
FFD	x	[−0.01,0.01]
	y	[−0.006,0.006]
	z	[−0.012,0.012]

For the optimization problem of DTMB-5415 ship, the objective function is the total resistance, which is defined as follows:

$$f_{\text{obj}} = R_t \quad \text{subject to} \quad -1\% \le \frac{S_0 - S}{S} \le 1\%,$$

$$-1.5\% \le \frac{\nabla - \nabla_0}{\nabla_0} \le 1.5\% \tag{13}$$

where S_0 is the wet surface of sample ships, ∇ is the displacement volume of the sample ships and ∇_0 is the displacement volume of the parent ship.

3.4 *Optimization results and analysis*

The resistance of sample data is obtained by the NMShip-SJTU and naoe-FOAM-SJTU. After that, a single high-fidelity Kriging surrogate model was constructed using 50 high-fidelity sample data. Among them, the input is the design variables, and the output is the resistance of sample data. At the same time, the maximum absolute error (MAE), average absolute error (AAE), mean square error (MSE) and coefficient of determination R^2 are used as indicators to discuss the accuracy of Kriging model constructed using different correlation functions and deterministic polynomials. The definition of R^2 is presented as

$$R^2 = 1 - \frac{\sum_i^n (\hat{f}_i - f_i^2)}{\sum_i^n (\overline{f}_i - f_i)^2} \tag{14}$$

where $\hat{f}$ is the prediction value of surrogate model, f is the CFD value of sample ships, $\overline{f}$ is the mean value of sample ships and n is the number of sample ships.

The results are shown in Table 5. In Table 5, corrgauss and corrspline represent the Gaussian correlation function and the spline correlation function in the Kriging model[20]. Regpoly 0, regpoly 1, regpoly 2 represents the zero-order deterministic polynomial, the first-order deterministic polynomial and the second-order deterministic polynomial in the Kriging model[20]. In Table 5, it can be seen that when the correlation function is the spline correlation function and the polynomial is the quadratic deterministic polynomial, the error is the smallest. Therefore, the Kriging surrogate model is constructed by combining the spline correlation function and the quadratic deterministic polynomial (corrgauss-repoly 2).

Table 5 Error analysis of Kriging model

	Regpoly 0	Regpoly 1	Regpoly 2	
Corrgauss	0.3700	0.4077	0.2774	AAE
	2.7968	2.0269	0.7691	MAE
	0.5835	0.5541	0.3432	MSE
R^2	0.9173	0.9254	0.9612	-
Corrspline	0.3682	0.3752	0.2819	AAE
	2.9480	2.1354	0.7761	MAE
	0.5986	0.5350	0.3508	MSE
R^2	0.9130	0.9305	0.9601	-

At the same time, when constructing a multi-fidelity deep neural network surrogate model, the number of low-fidelity data is 50. Among them, the input is the design variable values corresponding to the sample ships, and the output is the resistance of DTMB-5415 evaluated by potential flow solver. The high-fidelity neural network input is the design variable values of the sample ships and the resistance value of the sample ships predicted by the low-fidelity neural network. The output is the high-fidelity CFD evaluation results. To evaluate how many groups of high-fidelity sample data can achieve the best accuracy of the surrogate model, 60 high-fidelity sample data are obtained. Among them, 50 high-fidelity data which are the same as the data for constructing the Kriging model are used for neural network training, and 10 high-fidelity data are used to verify the accuracy of MFDNN surrogate model. The coefficient of determination R^2 is used as an indicator to discuss the number of high-fidelity samples. The results are shown in Table 6.

It can be seen from Table 6 that the R^2 shows a trend of increasing first and then decreasing. In the initial stage, due to the existence of a large number of low-fidelity sample data, although the low-fidelity

Table 6 Accuracy analysis of MFDNN model

Num of sample points	10	15	20	25	30	35	40	45	50
R^2	0.8032	0.8893	0.9492	0.9539	0.9694	0.9011	0.9142	0.8915	0.8824

Table 7 Comparison of optimal results

	Value of design variables					R_t			
	α_{1f}	α_{1a}	x	y	z	Prediction/N	CFD/N	Prediction error/%	Reduction ratio/%
Initial	0	0	0	0	0	-	44.66	-	-
Opt-K	0.016	0.016	0.01	0.006	0.0120	40.82	41.50	1.67	7.08
Opt-MFDNN	0.016	0.009	–0.01	0.006	0.0085	41.08	41.02	1.46	8.15

neural network model can predict the overall trend, the number of fused high-fidelity is small, which makes the accuracy low. When the number of high-fidelity data increases, high-fidelity data and low-fidelity data cooperate with each other to construct an accuracy surrogate model. However, when the high-fidelity data are further increased, the low-fidelity data are gradually covered by more high-precision samples, making it difficult for low-fidelity data to play. Therefore, it will eventually basically tend to the surrogate model constructed by pure high- fidelity data. In other words, when the total number of low-fidelity data is determined, the number of high-fidelity data has a smaller range, which makes the MFDNN surrogate model more accurate. On this basis, 50 groups of low-fidelity samples and 30 groups of high-fidelity samples are selected to construct a MFDNN surrogate model.

According to above analysis, the Kriging model and the MFDNN surrogate model are constructed. On this basis, the single-objective genetic algorithm is used to search for the optimal solution.

The design variables and optimization results corresponding to the two optimal hulls are shown in Table 7. To facilitate expression, we refer to the optimal hull obtained from the Kriging model as Opt-K and the optimal hull obtained from the MFDNN surrogate model as Opt-MFDNN. As shown in Table 7, compared with the initial hull, the resistance of Opt-MFDNN is reduced by 8.15%, and the resistance of Opt-K is reduced by 7.08%. Besides, comparing the predicted value and calculated value of the optimal hulls, the accuracy of MFDNN surrogate model is higher. Therefore, the MFDNN surrogate model can obtain better results using fewer high-fidelity data.

In addition, the evaluation time for one low-fidelity data is 0.25 h, while the evaluation time for one high-fidelity data is 43.9 h. Therefore, the total time of Kriging model is 2 195 h, and the MFDNN surrogate model is 1 329.5 h. By comparing the evaluation time of the two surrogate model, it can be found that the multi-fidelity deep neural network surrogate model requires less construction time, which improves the optimization efficiency by 39.43%. In addition, the accuracy of the MFDNN surrogate model is higher, so the multi-fidelity deep neural network offers more advantages.

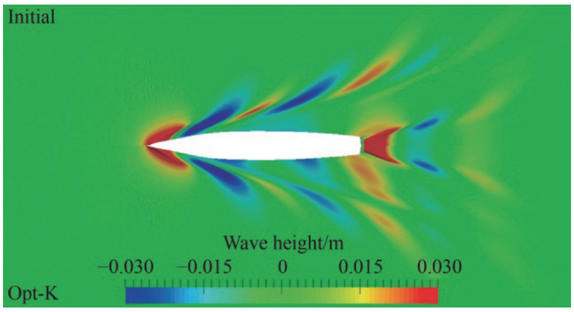

Fig. 10 Comparison of wave elevation between the Opt-K and initial hulls

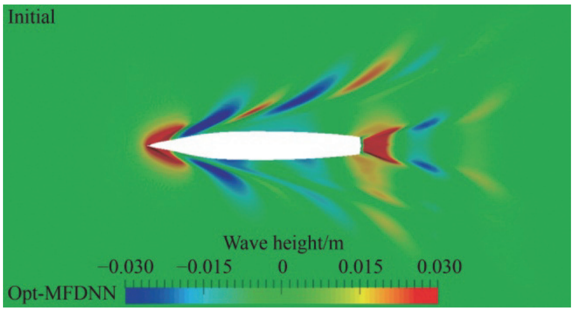

Fig. 11 Comparison of wave elevation between the Opt-MFDNN and initial hulls

Figures 10, 11 show the comparison of free surface wave evaluation between the two optimal hulls and the initial hull. From Figs. 10, 11, it can be seen that the overall phase of the bow wave system of the two optimal hulls is shifted backward due to the modification of the cross-sectional area curve using the shifting method. Compared with the initial hull, the free surface wave-making of the two optimal hulls has been improved.

Figure 12 is the bodylines comparison results between initial and optimal hulls. For the Opt-K hull, the volume of the sonar cover decreases and moves up as a whole, and the cross section of the rear half of the ship has a large translation range. In comparison, for the Opt-MFDNN hull, the volume of the sonar cover increases, but it also moves up as a whole. In addition, the cross section of the rear half of Opt-MFDNN hull has a small shifting range the. The detailed design variables of the two optimal hulls are shown in Table 7

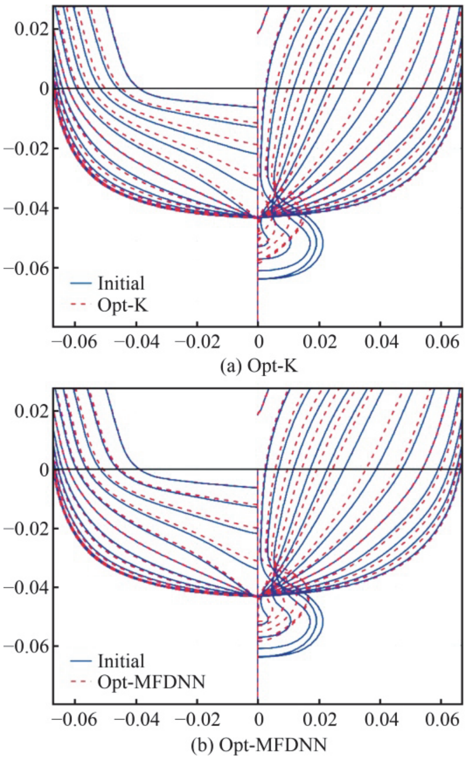

Fig. 12 Bodylines comparison of initial and optimal hulls

4. Conclusions

In this paper, a new hull form optimization framework based on multi-fidelity deep neural network is proposed. Firstly, the optimization framework is tested by mathematical function. Then, the optimization problem of DTMB-5415 resistance is carried out using the MFDNN surrogate model and the Kriging model. The conclusions are as follows:

(1) The optimization framework proposed in this paper can use fewer high-fidelity samples and combine more low-fidelity samples to construct a multi-fidelity surrogate model with higher accuracy, which can be used for hull form optimization.

(2) The multi-fidelity deep neural network surrogate model can take into account both efficiency and accuracy, and the resistance of the optimal hull is improved by 8.15%. The resistance of the Kriging model optimization results only improved by 7.08% when only high-fidelity data were used. And the multi-fidelity deep neural network model uses only 30 sets of high-fidelity data, and the optimization efficiency is greatly improved by 39.43%.

Conflict of interest

All authors declare that there are no other competing interests.

References

[1] Ni Q., Ruan W., Li S. et al. Multiple speed integrated optimization design for a SWATH using SBD technique [J]. *Journal of Marine Science and Technology*, 2020, 25: 185-195.

[2] Wang P., Feng Y., Chen Z. et al. Study of a hull form optimization system based on a Gaussian process regression algorithm and an adaptive sampling strategy, Part I: Single-objective optimization [J]. *Ocean Engineering*, 2023, 279: 114502.

[3] Sun T., Chen G., Yang S. et al. Design and optimization of a bio-inspired hull shape for AUV by surrogate model technology [J]. *Engineering Applications of Computational Fluid Mechanics*, 2021, 15(1): 1057-1074.

[4] Miao A., Wan D. Hull form optimization based on an NM+ CFD integrated method for KCS [J]. *International Journal of Computational Methods*, 2020, 17(10): 2050008.

[5] Jakobsson S., Patriksson M., Rudholm J. et al. A method for simulation based optimization using radial basis functions [J]. *Optimization and Engineering*, 2010, 11: 501-532.

[6] Ao Y., Duan H., Li S. An integrated-hull design assisted by artificial intelligence-aided design method [J]. *Computers and Structures*, 2024, 297: 107320.

[7] Wang S., Kim Y. CFD-based hull optimization in calm water using adaptive grid deformation method [J]. *Journal of Hydrodynamics*, 2024, 36(2): 241-262.

[8] Feng Y., Chen Z., Dai Y. et al. Multidisciplinary optimization of an offshore aquaculture vessel hull form based on the support vector regression surrogate mode l [J]. *Ocean Engineering*, 2018, 166: 145-158.

[9] Tahara Y., Peri D., Campana E. F. et al. Single-and multiobjective design optimization of a fast multihull ship: numerical and experimental results [J]. *Journal of Marine Science and Technology*, 2011, 16: 412-433.

[10] Liu X., Zhao W., Wan D. Hull form optimization based on calm-water wave drag with or without generating bulbous bow [J]. *Applied Ocean Research*, 2021, 116: 102861.

[11] Huang F., Wang L., Yang C. Hull form optimization for reduced drag and improved seakeeping using a surrogate-based method [C]. *ISOPE International Ocean and Polar Engineering Conference. ISOPE*, Hawaii, USA, 2015.

[12] Diez M., Campana E. F., Stern F. Stochastic optimization methods for ship resistance and operational efficiency via CFD [J]. *Structural and Multidisciplinary Optimization*, 2018, 57: 735-758.

[13] Coppedè A., Gaggero S., Vernengo G. et al. Hydrodynamic shape optimization by high fidelity CFD solver and Gaussian process based response surface method [J]. *Applied Ocean Research*, 2019, 90: 101841.

[14] Liu Z., Liu X., Wan D. Wigley hull design optimization based on artificial neural network and genetic algorithm [C]. *ISOPE Pacific/Asia Offshore Mechanics Symposium. ISOPE*, Dalian, China, 2020.

[15] Hou Y. Hull form uncertainty optimization design for minimum EEOI with influence of different speed perturbation types [J]. *Ocean Engineering*, 2017, 140:

66-72.
[16] Liu X., Zhao W., Wan D. Multi-fidelity Co-Kriging surrogate model for ship hull form optimization [J]. *Ocean Engineering*, 2022, 243: 110239.
[17] Liao P., Song W., Du P. et al. Multi-fidelity convolutional neural network surrogate model for aerodynamic optimization based on transfer learning [J]. *Physics of Fluids*, 2021, 33(12):127121.
[18] Kennedy M. C., O'Hagan A. Predicting the output from a complex computer code when fast approximations are available [J]. *Biometrika*, 2000, 87(1): 1-13.
[19] Forrester A. I. J., Sóbester A., Keane A. J. Multi-fidelity optimization via surrogate modeling [J]. *Proceedings of the royal society A: Mathematical, Physical and Engineering Sciences*, 2007, 463(2088): 3251-3269.
[20] Liu X., Wan D., Lei L. Multi-fidelity model and reduced-order method for comprehensive hydrodynamic performance optimization and prediction of JBC ship [J]. *Ocean Engineering*, 2023, 267: 113321.
[21] Scholcz T., Klinkenberg J. Hull-shape optimisation using adaptive multi-fidelity Kriging [C]. *NATO-AVT-354 workshop on multi-fidelity methods for military vehicle design*, Varma, Bulgaria, 2022.
[22] Zhang X., Xie F., Ji T. et al. Multi-fidelity deep neural network surrogate model for aerodynamic shape optimization [J]. *Computer Methods in Applied Mechanics and Engineering*, 2021, 373: 113485.
[23] Sun D., Wang Z., Qu F. et al. A deep learning based prediction approach for the supercritical airfoil at transonic speeds [J]. *Physics of Fluids*, 2021, 33(8):086109.
[24] Han B., Huang W. Active control for drag reduction of turbulent channel flow based on convolutional neural networks [J]. *Physics of Fluids,* 2020, 32(9): 095108.
[25] Meng X., Karniadakis G. E. A composite neural network that learns from multi-fidelity data: Application to function approximation and inverse PDE problems [J]. *Journal of Computational Physics*, 2020, 401: 109020.
[26] Perdikaris P., Raissi M., Damianou A. et al. Nonlinear information fusion algorithms for data-efficient multi-fidelity modeling [J]. *Proceedings of the Royal Society A: Mathematical, Physical and Engineering Sciences*, 2017, 473(2198): 20160751.